TRANSACTIONS OF THE INSTITUTE OF FLUID-FLOW MACHINERY

No. 129, 2015, 111–141

JUDYTA FELICJANCIK[a,b] [1], PAWEŁ ZIÓŁKOWSKI[a,b] and JANUSZ BADUR[a]

An advanced thermal-FSI approach of an evaporation of air heat pump

[a] *Energy Conversion Department, The Szewalski Institute of Fluid-Flow Machinery of the Polish Academy of Sciences, Fiszera 14, 80-231 Gdańsk, Poland*

[b] *Conjoint Doctoral School at the Faculty of Mechanical Engineering, Gdańsk University of Technology, Narutowicza 11/12, 80-233 Gdańsk, Poland*

Abstract

The paper presents selected problems of numerical modelling of an advanced thermal-FSI (Fluid solid interaction) approach of evaporator of air heat pump. The example of a fin-tube evaporator has been studied, focusing on obtaining the heat exchanger characteristics applying two-phase flow model for the in-tube refrigerant flow. Special attention is given to heat transfer between separated medium for different air velocity and changed refrigerant mass flow in-tube.

Keywords: CFD modeling; Evaporator; Fin-tube heat exchanger; Heat transfer

Nomenclature

A	–	heat transfer area, m^2
C	–	constant
c	–	specific heat, J/(kg K)
D	–	IQT dissipation operator
d	–	diameter, m

[1] Corresponding author. E-mail address: judyta.felicjancik@imp.gda.pl

e	–	total energy composed of internal and kinetic energy, $e = c_v T + \frac{1}{2} v_i v_j$, kJ/kg
G	–	source component of k operator
H	–	Hamiltonian
h	–	specific enthalpy, kJ/kg
$\hbar$	–	modified Planck constant
k	–	turbulent kinetic energy
L	–	tube length, m
$\dot{m}$	–	mass flow rate, kg/s
p	–	pressure, N/m^2 ≡Pa
Pr	–	Prandtl number
Pr_T	–	turbulent Prandtl number ($\mathrm{Pr}_T = 0.85$ – at the wall)
$\dot{Q}$	–	heat flux, W
$\dot{q}$	–	specific heat flux, W/m^2
Re	–	Reynolds number
T	–	temperature, K
t	–	time
T_r	–	trace of matrix
U^*	–	nondimensional velocity
w	–	axial velocity, m/s
x	–	vapour quality
y	–	wetness degree
y^*	–	layer

Notation for vector quantities

$\vec{b}$	–	mass force, $\vec{b} = b_i$, m/s^2
$\vec{F}$	–	flux
$\overleftrightarrow{G}$	–	Maxwell thermal transpiration
$\vec{g}$	–	thermal diffusion
$\vec{h_\eta}$	–	Rankine entropy flux
$\overleftrightarrow{I}$	–	Unit tensor (Gibbs' idemfactor), $\{i, j = x, y, z\}$, $\overleftrightarrow{I} = \delta_{ij}\vec{e_i} \otimes \vec{e_j} = \vec{e_x} \otimes \vec{e_x} + \vec{e_y} \otimes \vec{e_y} + \vec{e_z} \otimes \vec{e_z}$
$\vec{J_k}$	–	diffusive flux of k, $\vec{J_k} = J_i^k \vec{e_i}$
$\vec{J_\varepsilon}$	–	diffusive flux of ε, $\vec{J_\varepsilon} = J_i^\varepsilon \vec{e_i}$
$\vec{n}$	–	normal vector
$\vec{v}$	–	fluid velocity vector, $\vec{v} = u\vec{e}_x + v\vec{e}_y + w\vec{e}_z = v_i\vec{e_i}$
$\rho\vec{v} \otimes \vec{v}$	–	convective momentum flux, $\rho\vec{v} \otimes \vec{v} = \rho v_i v_j \vec{e_i} \otimes \vec{e_j}$
$\overleftrightarrow{\tau}^c$	–	total, irreversible momentum flux, $\overleftrightarrow{\tau}^c = \overleftrightarrow{\tau} + \overleftrightarrow{R} = \tau_{ij}\vec{e_i} \otimes \vec{e_j} + R_{ij}\vec{e_i} \otimes \vec{e_j}$
$\vec{q}^c$	–	total heat flux, $\vec{q}^c = \vec{q} + \vec{q}^t = q_i\vec{e_i} + q_i^t\vec{e_i}$
S_k, S_ε, S_e	–	k, ε and e sources

Constants

A	–	Van Driest's constant ($A = 26$)
κ	–	von Karman's constant ($\kappa = 0.42$)
E	–	wall function constant ($E = 9.793$)

Greek symbols

α	–	heat transfer coefficient, $\mathrm{W/(m^2\,K)}$
β	–	volume expanation, $1/\mathrm{K}$
δ_{ij}	–	Kronecker delta
ε	–	indicator of energy effectiveness, rate of dissipation of turbulent kinetic energy
η	–	specific entropy, $\mathrm{kJ/(kg\,K)}$
κ	–	volume turbulent viscosity
λ	–	thermal conductivity, $\mathrm{W/(m\,K)}$
μ	–	dynamic viscosity, $\mathrm{kg/m\,s}$
ν	–	kinematic viscosity, $\mathrm{m^2 s}$
ρ	–	density, $\mathrm{kg/m^3}$
σ	–	entropy production
τ	–	scalar time constant for IQT

Subscripts

A	–	surface
air	–	air
$chem$	–	chemical
e	–	node of a finite volume
e-m	–	electromagnetical
F	–	flux
FVM	–	Finite Volume Method
f	–	fluid
$heat$	–	thermal
int	–	internal
l	–	liquid
M	–	temperature in the boundary layer
$mass$	–	mass
$mech$	–	mechanical
N	–	overpressure
p	–	pressure constant
P	–	distance between neighbouring pressure-measurement pipes
S	–	saturation temperature
v	–	vapour, volume constant
W	–	wal temperature
w	–	wall
’	–	saturated liquid entropy at s given pressure
”	–	saturated vapour entropy at s given pressure

1 Introduction

Despite the significant progress lately made in the research on the heat transfer, the physical mechanism for energy transport in this process is not sufficiently known, e.g., [9, 34]. The main reason for this are significant difficulties on the turbulent boundary layer, especially in its development at areas of flow separation, re-adjoining and relaminarisation. Unknown are also, to a satisfactory extent, mechanisms of enhanced energy transport by heat in areas of the laminar-turbulent transitions induced by various obstacles in the fluid. It is only known, that various locations and configurations of obstacles promote turbulence characterized with a large scale periodicity relevant to obstacles spacing, their dimensions and the velocity of working fluid [18, 50].

Another reason worth to be mentioned is the complex nature of heating. In the literature there is no one common mechanism responsible for transport of mass, energy, momentum during heating. Therefore, according to many different theoretical view point we have a lot of governing equations related to the temperature field being a fundamental unknown. Among them the most popular are (see: Gyftopoulos, Beretta [28], Cano-Andrade *et al.* [16], Bejan [10, 11], Feidt [20]:

- intrinsic quantum thermodynamic (IQT) [16]:

$$\frac{d\rho}{dt} = -\frac{i}{\hbar}\left[H,\rho\right] - \left(\frac{1}{\tau_A} D_A \oplus \rho_F + \frac{1}{\tau_F}\rho_A \oplus D_F\right). \tag{1}$$

  Let recall some basic elements of above governing equations of thermal motion. In IQT Eq. 1 the evolution of density state operator of thermal motion is given by two terms. The first term on the right-hand side describes the unitary Hamiltonian dynamics of the system and the second the non-Hamiltonian dissipation dynamics. The operator $[H,\rho] = H\rho - \rho H$ is the commutator between Hamiltonian and density state operator, and $\rho_A = Tr_F\rho$; $\rho_F = Tr_A\rho$ are reduced state operators. Additionally, τ_A and τ_F are characteristic times for subsystems A (internal) and F (external). Important feature of the IQT model is that it can exactly describe the locally perceived energy and locally preserved entropy [16] – it means that having these local observables one can defines – using the Gyftopoulos-Beretta and von Neumann definitions – both energy and entropy for the overall system.

- Locally maximum entropy production principle (LMEPP)[1] [10]

$$\frac{\partial \sigma}{\partial T} + \mathrm{div}\Big(\frac{\partial \sigma}{\partial \vec{g}} - \mathrm{div}\frac{\partial \sigma}{\partial \overset{\leftrightarrow}{G}}\Big) = 0\,. \tag{2}$$

  Equation (2) is known to be governing equation of LMEPP (Bejan [10]) and is generously based on the notion of entropy production σ. Assuming that this entropy production depends on the temperature gradient $\vec{g} = \mathrm{grad}T$ [thermal diffusion] and the second gradient $\overset{\leftrightarrow}{G} = \mathrm{grad}\,\vec{g}$ (Maxwell thermal transpiration) we can reinterpret Eq. (2) to be a Euler-Lagrange variational condition for maximal entropy production [13].

- Balance of entropy [3]:

$$\frac{\partial}{\partial t}(\rho\eta) + \mathrm{div}(\rho\eta\vec{v} + \vec{h}_\eta) + \rho\sigma = 0\,. \tag{3}$$

  Equation (3) presents the most problematic equation of the whole classical field theory – the balance of specific entropy η. Here the continuum density is denoted by ρ, the specific momentum vector by $\vec{v}$ and the Rankine entropy flux by $\vec{h}_\eta$. As above the specific entropy production is denoted by σ.

- Balance of energy [7]:

$$\frac{\partial}{\partial t}(\rho e) + \mathrm{div}(\rho e\vec{v}) = \mathrm{div}(\vec{F}_{mech} + \vec{F}_{heat} + \vec{F}_{chem} + \vec{F}_{e-m} + \vec{F}_{mass} + \ldots)\,. \tag{4}$$

  In practice, the balance of Eq. (4) is a governing equation for the field of temperature $T(\vec{x},\, t)$. According to the principle of producing of energy 'ex nihilo' in Eq. (4) there is no internal sources of energy and the changing of energy e is governed only by energy fluxes $\vec{F}_a, a = mech, heat, chem, e-m, mass, \ldots$. The most important for describing of thermal motion dynamics is the Stokes-Rankine heating energy flux $\vec{F}_{heat}$, frequently denoted in the literature by letter $\vec{q}$. By the Rankine formula : flux $\vec{F}_{heat} = T\vec{h}_\eta$ the equation of energy is indirectly connected with the thermal equation of motion or the balance

[1] In this case, a general formulation of balance equation was used in so-called non-indexed notation which denotes vector with an arrow over a symbol: $\vec{g}$, and tensors with double arrow: $\overset{\leftrightarrow}{G}$.

of entropy, therefore, in numerical problems, the balance of energy leads to determine the temperature field [6, 7].

The above four governing equations for the temperature field are only examples of efforts of scientific community to understand the fundamental behaviour of nature. For instance, balance of entropy and energy are in the core of explaining the transition between macroscopic and microscopic worlds [20]. Furthermore, there is no one common picture for describing complexity of types of communication phenomena. Thus, thinking on transport of heating across the solid-fluid contact layer one should consider an exact nature of a non-linear equation of thermal motion. The examples given above by Eqs. (1)–(4) are the most known – others, like 'steepest entropy ascent' (SEA), 'dissipative quantum dynamic' (DCD), etc., are under permanent efforts of scientific community [28].

1.1 Intensification of heat transfer in laminar-turbulent transition

Considering a three-dimensional (3D) mathematical modelling, the phenomenon of 'intensified' energy exchange must be slightly different described using a heat exchange 3D model for flow turbulized with various bluff bodies, various velocity, various medium etc. Since the modeling of turbulent flows with heat transfer focuses mainly on solving properly velocity field rather than temperature field, it is generally accepted that the influence of turbulence models for momentum on the solution is much greater than the influence of turbulence closures for energy equation which are usually simplified to an algebraic expressions [5, 23, 44].

The simplest way of turbulent heat flux modelling by meaning of employing a constant or varying turbulent Prandtl number, Pr_T, seems to be sufficient and economical not only for prediction of smooth pipe but a peculiarly shaped channel walls with troughs, edgings, fins, etc. Such a way of turbulent heat flux modelling is a direct succession of the so-called Reynolds analogy between turbulent heat and momentum transfer. Some authors [42] argue that more sophisticated models are needed, especially that it should be no more difficult and time consuming. However, in the following paper is based on developing a varying turbulent Prandtl number with own calibrated closure for more complicated geometry than a straight channel [5, 17].

Classic research indicates that the natural laminar-turbulent transition

surface is in a some proportion to the channel surface, whereas the area of induced laminar-turbulent transition is few orders of magnitude bigger. The second important factor influencing the level of induced heat exchange is the size of so-called turbulence spots depending on the size of coherent structures hitting the layer. The research reveals that the more compact the turbulence spot is, the deeper they penetrate the boundary layer and intensify the movement of heated fluid particles. Research also shows, that in the second case, that is with especially shaped walls of the heat-exchanging channel, the main mechanism for heat exchange intensification is the flow separation area behind the geometric obstacle disturbing the flow, flow laminarisation phenomena in the boundary layer as well as the transverse motion induced by longitudal vortices deeply penetrating the flow [40, 50, 52].

On the other hand, research indicates also that the heat exchange process in flow separation area has a character of fluid state relaxation in front of the obstacle. Thus, the boundary layer, developing in the area of splitting and rejoining should have a new structure defined as an relaxational, dissimilar to classical boundary layer in the confusor flows. A specific feature of that boundary layer is an immanent anisotropy of turbulent sublayer, which should not be omitted in mathematical models [18, 40, 52, 53]. Global information about heat transfer intensification provides the main parameters of heat exchanger. An example of research in the area of heat exchanger is presented in the next section.

1.2 Heat exchangers

Many studied have been carried out on modeling and experimental research thermoflow behaviours and prediction of heat exchanger characteristics. Gherasim *et al.* [24–26] has analyzed alike the temperature, the flow resistance and the stream of transferred heat in the plate heat exchanger (PHE) between fluids: water-water, water-oil. As research of Gherasim *et al.* has shown, the use of numerical calculations is justified because of the relatively low accuracy of the analytical calculations were obtained [26]. In [26], an experimental study on the bench was conducted, and later analytical calculations were compared with the results of the experiment. Then obtained results was secondly compared with another works results. In [25] there is shown, in a detailed way, a methodology for performed numerical calculations, with comparisons of the results for different methods. It is found, that the selection of the model depends on many factors, inter alia, the flow velocity, a nature of the flow or the fluid temperature. When the

models are calibrated inappropriate, the differences comes to 10% [24, 25].

The work of Jin *et al.* [30] presents a detailed numerical analysis of PHE with the distribution of velocity and temperature in canaliculus with fluid, emphasizing that this analysis is not doable in an experimental way. On the other hand study by Fernandes *et al.* [21] presents computational fluid dynamics (CFD) analysis of laminar flow in industrial heat exchangers, focusing on the effects of tortuosity and shape of the heat exchanger on the flow resistance, depending on the Reynolds number. In Abdulsayid's paper [1] there was studied two-dimensional geometry of the flow channel, in concept of the three profiles – types of incision in channel – triangular, rectangular and sinusoidal. It has been found that entering these inequalities often causes significant losses in flow, not compensated by increased coefficient of heat transmission. Kanaris *et al.* [31] presents CFD model validatied with his own experiment on a PHE, in order to optimize the geometry. Nusselt number and coefficient of friction were analyzed. Numerical calculations coincide with correlations and experimental results for the analyzed heat exchangers. Recently there also arise works about phase transformation of carbon dioxide (CO_2) and other low boiling coefficients in microchannels. In some paper both experimental work leading to the correlation [19, 29, 39] and articles presenting models often calibrated to experiment [39, 42, 43, 46] are presented.

This paper is devoted to the presentation of a model fin– and –tube evaporators, focusing on obtaining the heat exchanger characteristics of two-phase flow model for the in-tube refrigerant flow. According to that purpose, an advanced thermal-FSI approach in the 3D version has been used. Special attention is given to heat transfer between separated medium for different air velocity and different refrigerant mass flow rate in-tube. Methodology of heat transfer from work [5, 7] has been taken and developed in two-phase flow. Selected cases are analyzed in a full detail, showing the impact of air mass flow rate on the fin-tube temperature distributions. These phenomena are illustrated and discussed.

2 Mathematical and numerical modeling

Mathematical modeling of the problem of heat transfer intensification is, in general, a difficult task, as mathematical models should be reasonably easy transferable to numerical models that should be easy to implement and calibrate. Computational fluid dynamics (CFD), naturally joining mass,

momentum and energy equations into one common base for discretization and numerical solving, experienced a rapid development in 1970–1980s. In the last years tools allowing for description of each particular turbulent vortex bursting from an obstacle into channel boundary layer have also been developed. These tools, unfortunately, unsufficiently known, include direct numerical simulation (DNS) and large eddy simulation (LES) [5].

Mathematical and numerical bases of convective, turbulent heat transfer have been given in [5, 14, 18, 51]. The experience of numerous authors [5, 8, 9, 23, 33, 39, 45, 48, 49] proofs that, the practical application of numerical modeling to heat exchange phenomena emerges as an important and effective completion of extremely expensive experimental research. However, it should be stressed, that numerical simulation shall be reliable and trustworthy [5, 8, 48, 49] which is usually achieved with experimental verification at a laboratory site.

Numerical modeling with a Prandtl number closure implementation, is based on the commercial CFD code with conventional phenomenological mass, momentum and energy balance equations. As usual, in the case of turbulent flows, apart from molecular momentum and energy fluxes, turbulent momentum and energy fluxes appear, which must be modeled additionally. The most frequently tested in technical devices turbulent closure model is the two-equation k-ε model originally developed by Laudner and Spalding [38]. The original form of this model had served as a base for its different modifications as shown in [44, 45] and it has been adopted with small changes. However, a directional thermal anisotropy has been introduced in the turbulent heat flux. Therefore, computations presented in this paper use the k-ε turbulence model with a variable Prandtl number Pr_T as a starting model for correctness and calibrations [5, 17].

3 The modeled system

A heat exchanger accepted for our study is a finned-tube evaporator. The flow diagram within the exchanger is shown in Fig. 1. Coefficients in finned-tube heat exchangers are chosen such that the value of convective heat-transfer coefficient on one side of the wall, in comparison with the value of heat transfer coefficient on the other side, is low. A typical example is a heat exchanger in which heating medium is vapour of CO_2 and air is heated or when the cooling medium is evaporating CO_2 and air is cooled [2].

In the considered case the refrigerant, cooperating with the air, is carbon

dioxide, and their basic physical properties are shown in Tab. 1. For the air we have given temperature parameters of 273 K and 285 K (see Fig. 2). In contrast for carbon dioxide the saturation temperature parameters of 273 K is given, both for the liquid (l) and vapour (v) (see Fig. 2). Carbon dioxide is characterized not only by high-pressure operation, but also by the high heat transfer coefficients. It belongs to modern low-boiling heat-transfer medium, despite the fact that its properties have been used much earlier. Nowadays material and design possibilities can contribute to this. For the calculation it has been assumed to make an exchanger elements of copper, which is characterized by very good thermal properties, but its disadvantage is the relatively high weight and high cost.

Table 1: Physical properties of the analyzed medium [15].

Properties	Symbol	Unit	Value of properties	
			Air	Carbon dioxide
Density	ρ	kg/m^3	$1.293_{(0\,^\circ\mathrm{C})}/1.293_{(12\,^\circ\mathrm{C})}$	$927.43_{(l)}/927.43_{(v)}$
Thermal conductivity	λ	W/m K	$2.44\times10^2_{(0\,^\circ\mathrm{C})}/2.53\times10^2_{(12\,^\circ\mathrm{C})}$	$0.047_{(l)}/20.85\times10^3_{(v)}$
Heat capacity	c_p	kJ/kg K	1.005	$2.41_{(l)}/1.787_{(v)}$
Dynamic viscosity	μ	N s/m^2	$17.2\times10^6_{(0\,^\circ\mathrm{C})}/17.7\times10^6_{(12\,^\circ\mathrm{C})}$	$98.7\times10^6_{(l)}/15.44\times10^6_{(v)}$

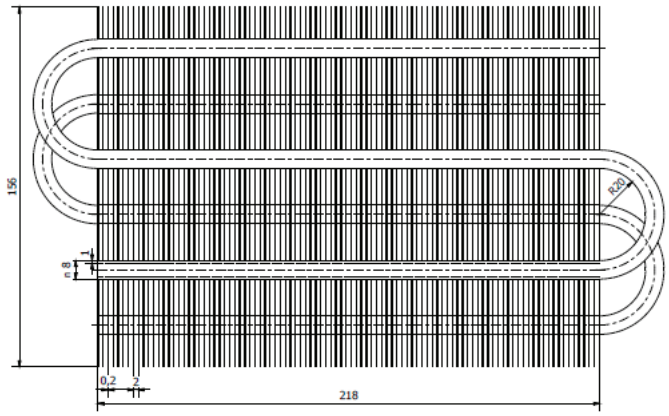

Figure 1: The dimensions of analyzed heat exchanger.

Figure 1 presents the characteristic dimensions of the heat exchanger model,

assumed for the analysis. One hundred thin fins are placed in parallel to each other at distance of of 2 mm. Through the interlamellar space flows the air. Between the fins is led twice recycled tube inner diameter of $d = 6$ mm. On the wall's side, symmetry and periodicity conditions were set, so that the element can be regarded as a section of the heat exchanger.

4 Governing equations

The above stated problem of heat exchange intensification in fluid flow channel was solved as a coupled heat exchange problem between solid and fluid. For a complete temperature field coupling, the energy equation should be solved both for the solid body (copper pipe 3×218 mm long with 1 mm thick wall) and for the fluid – medium running in the channel. It is assumed that deformations of the copper pipe intercepting vapour condensation heat at the outer side of the pipe and giving it out at the inner wall of the pipe, are negligibly small thus allowing for omitting momentum and mass balance consideration for the solid body.

4.1 Mass balance (continuity) equation [3]

$$\frac{\partial}{\partial t}\rho + \frac{\partial}{\partial x_i}(\rho v_i) = 0\,, \tag{5}$$

where:

- ρ – fluid density, $\rho = \rho(x_i, t)$, generally dependent on time and location,
- $\vec{v}$ – fluid velocity, $\vec{v} = v_i\vec{e}_i$, $i = x, y, z$,
- x_i – coordinates used at finite volume method, $i = 1, 2, 3$ (structural mesh) or $i = x, y, z$ (nonstructural mesh).

4.2 Momentum balance equation [5, 37]

$$\frac{\partial}{\partial t}(\rho v_i) + \frac{\partial}{\partial x_j}(\rho v_i v_j + p\delta_{ij}) = \frac{\partial}{\partial x_j}(\tau_{ij} + R_{ij}) + \rho b_i\,, \tag{6}$$

where:

- p – thermodynamic pressure,
- δ_{ij} – Kronecker delta [27, 32],
- τ_{ij} – viscous stress flux components,
- R_{ij} – Reynolds turbulent stress,
- b_i – mass force of Earth gravity, $b_i = -9.81\,\delta_{iz}$.

4.3 Energy balance equation

Energy balance equation can be written in the so-called 'conservative' form

$$\frac{\partial}{\partial t}(\rho e) + \frac{\partial}{\partial x_i}(\rho e v_i + p v_i) = \frac{\partial}{\partial x_i}\big(q_i + q_i^t + \tau_{ij} v_j + R_{ij} v_j\big) + \rho b_i v_i \,, \qquad (7)$$

where additionally, the following notation was used:

- e – internal and kinetic energy, $e = u + \frac{\vec{v}^2}{2}$,
- u – internal energy, $u = c_v T$,
- q_i – molecular heat flux,
- q_i^t – turbulent heat flux.

4.4 Equation for turbulent kinetic energy evolution k

The five balance equation (that is one mass balance equation, three momentum balance equations and one energy balance equation) complete two evolution equation for parameters defining turbulence, first is [38]:

$$\frac{\partial}{\partial t}(\rho k) + \frac{\partial}{\partial x_i}(\rho k v_i) = \frac{\partial}{\partial x_i}(J_i^k) + \rho S_k \,. \qquad (8)$$

4.5 Equation for turbulent dissipation energy evolution ε

Second equation for turbulence evolution k-ε can be written as:

$$\frac{\partial}{\partial t}(\rho \varepsilon) + \frac{\partial}{\partial x_i}(\rho \varepsilon v_i) = \frac{\partial}{\partial x_i}(J_i^\varepsilon) + \rho S_\varepsilon \,, \qquad (9)$$

where: J_i^k, J_i^ε – diffusive flux of k and diffusive flux of ε with sources S_k, S_ε respectively (various definitions of different authors exist in literature) [3].

The seven equations given above define seven fundamental model unknowns: density ρ, velocity $\vec{v}$, temperature T, kinetic energy of turbulence k and turbulence dissipation ε. In order to solve these equations, additionally should be introduced caloric and thermic state equations for internal energy description as well as the Navier-Stokes constitutive equation (defining molecular stresses), the Fourier-Kirchhoff equation (defining molecular heat flux) together with closures for Reynolds turbulent stresses, R_{ij}, turbulent heat flux q_i^t and equations defining J_i^k, J_i^ε fluxes and S_k, S_ε sources used in evolution Eqs. (8) and (9).

4.6 The set of CFD balance equations

The set of balance and evolution equations given above in Cartesian coordinates has a sufficient form only if nonstructural discretization grids are used for its discretization. However, in case of regular geometries structural grids should be used, which require curvilinear coordinates description. In this case, a general formulation of balance equation was used in so-called nonindexed notation which denotes vector with an arrow over a symbol: $\vec{v}$, and tensors with double arrow, $\overset{\leftrightarrow}{\tau}$. Dyadic found in Eq. (10) is further denoted as $\vec{v} \otimes \vec{v}$ [32]. To maximize the use of the easily implementable matrix calculus, the starting point for CFD computation is to formulate universal set of mass, momentum and energy balance equations for the fluid, completed with equations for turbulence evolution k-ε in the form of [3]

$$\frac{\partial}{\partial t}\begin{Bmatrix} \rho \\ \rho\vec{v} \\ \rho e \\ \rho k \\ \rho\varepsilon \end{Bmatrix} + \operatorname{div}\begin{Bmatrix} \rho\vec{v} \\ (\rho\vec{v}\otimes\vec{v}) + p\overset{\leftrightarrow}{I} \\ (\rho e + p)\vec{v} \\ \rho\vec{v}k \\ \rho\vec{v}\varepsilon \end{Bmatrix} = \operatorname{div}\begin{Bmatrix} 0 \\ \overset{\leftrightarrow}{\tau^c} \\ \overset{\leftrightarrow}{\tau^c}\,\vec{v} + \vec{q}^c \\ \vec{J}_k \\ \vec{J}_\varepsilon \end{Bmatrix} + \begin{Bmatrix} 0 \\ \rho\vec{b} \\ \rho S_e \\ \rho S_k \\ \rho S_\varepsilon \end{Bmatrix}. \tag{10}$$

For each finite volume of the computational grid seven equations are solved (one for mass, energy, k and ε transport balance equation and three momentum balance equations). For the solid body only one equation is solved in the form of heat conduction equation neglecting wall deformations and thermal wall deformation.

4.7 Molecular flux of momentum

The fundamental momentum flux due to molecular viscosity found in Eq. (6) is called viscous stress tensor and defined by Navier-Stokes constitutive equation [35]:

$$\tau_{ij} = \mu\Big(\frac{\partial v_i}{\partial x_j} + \frac{\partial v_j}{\partial x_i}\Big) - \frac{2}{3}\mu\frac{\partial v_k}{\partial x_k}\delta_{ij}\,, \tag{11}$$

where the only one material constant can be found – dynamic viscosity, μ.

4.8 Turbulent momentum flux

Turbulent momentum flux, also called the Reynolds stress tensor is defined in an analogical form [5]

$$R_{ij} = \mu_T\Big(\frac{\partial v_i}{\partial x_j} + \frac{\partial v_j}{\partial x_i}\Big) - \frac{2}{3}\Big(\rho k + \mu_T \frac{\partial v_k}{\partial x_k}\Big)\delta_{ij}\,. \tag{12}$$

In Eq. (12), μ_T and k play the role of turbulent viscosities (shear and volume, respectively). Turbulent viscosity coefficient η_T is connected with fundamental turbulence parameters k-ε (according to the two scales Launder-Spaling model [38])as follows:

$$\mu_T = C_\mu \rho \frac{k^2}{\varepsilon}\,, \tag{13}$$

where C_μ is a constant which needs to be calibrated for specific type of geometry, independent of kind of fluid (water, air).

4.9 Molecular heat flux

The molecular heat flux is defined by Fourier-Kirchhoff classical constitutive equation in the form of [5]

$$q_i = \lambda \frac{\partial}{\partial x_i} T\,, \tag{14}$$

where λ is a molecular heat conductivity coefficient defined with relation to the molecular viscosity coefficient as

$$\lambda = \frac{c_p \mu}{\mathrm{Pr}}\,, \tag{15}$$

whereas c_p denotes specific heat under constant pressure and Pr nondimensional Prandtl number.

4.10 Turbulent heat flux

The turbulent momentum flux can be described in a form analogical to the turbulent heat transport, which can further be transformed, using Fourier law, into

$$q_i^t = \lambda_T \frac{\partial}{\partial x_i} T\,, \tag{16}$$

where λ_T is the turbulent heat conductivity coefficient defined in analogy with the molecular thermal conductivity coefficient (so-called algebraic Wolfstein closure) as

$$\lambda_T = \frac{c_p \mu_T}{\mathrm{Pr}_T} \,. \tag{17}$$

The turbulent Prandtl number is, for most cases, not a constant [44]. As we enter into the wall layer, it becomes variable. In Eq. (17) a new turbulent viscosity coefficient μ_T is also found, expressed as a function of two parameters: turbulent kinetic energy, k, and the rate of the turbulence energy dissipation, ε, responsible for momentum transport.

4.11 Two equation k-ε turbulence model

Diffusive fluxes J_i^k and, J_i^ε forming a part of the diffusive flux in Eqs. (8) and (9) are described with [3]

$$J_i^k = \Big(\mu + \frac{\mu_T}{\sigma_k}\Big)\frac{\partial}{\partial x_i} k \,, \tag{18}$$

$$J_i^\varepsilon = \Big(\mu + \frac{\mu_T}{\sigma_\varepsilon}\Big)\frac{\partial}{\partial x_i} \varepsilon \,, \tag{19}$$

where σ_k and σ_ε found in Eqs. (18) and (19) are constants which require calibration. An important issue is to define the components of vector S for k and ε evolution equations denoted as S_k – for k source and S_ε – for ε source in Eqs. (8) and (9). These components can be written as [22]

$$\rho S_k = G_k + G_b - \rho\varepsilon \tag{20}$$

or, as so-called the Laudner closure for source:

$$\rho S_\varepsilon = C_{1\varepsilon}\frac{\varepsilon}{k}\left\{G_k + (1 - C_{3\varepsilon})G_b\right\} - C_{2\varepsilon}\rho\frac{\varepsilon^2}{k} \,, \tag{21}$$

where G_k stands for the source of k related turbulent stresses, noting that

$$G_k = -\overline{\rho' v_i' v_j'}\,\frac{\partial v_j}{\partial x_i} = R_{ij}\frac{\partial}{\partial x_i} v_j \,, \tag{22}$$

and G_b is the source of k related to bouyant anisotropic advection:

$$G_b = \beta b_i \frac{\mu_T}{\mathrm{Pr}_T}\frac{\partial T}{\partial x_i} \,, \tag{23}$$

where b_i is a mass force, and coefficient of the thermal volume expansion β results from

$$\beta = -\frac{1}{\rho}\Big(\frac{\partial \rho}{\partial T}\Big)_P . \tag{24}$$

In Eqs. (18)–(24) a number of constants serving as k and ε evolution equation closures are found, which needs their value to be determined experimentally. For the further analysis, their values are taken as follows [22]:

$$C_{1\varepsilon} = 1.44,\ C_{2\varepsilon} = 1.92,\ C_{3\varepsilon} = 0.2,\ C_{\mu} = 0.09,\ \sigma_k = 1.0,\ \sigma_{\varepsilon} = 1.3.$$

Despite the above described model simulates sufficiently well the volume turbulence phenomena, it needs additional near wall corrections in the form of so-called wall functions. At the inlet to the channel, values of both k and ε have also been assumed.

4.12 Standard wall functions

The presence of walls naturally influences the flow of fluid. Within the fluid layer located in direct vicinity of the wall (called the wall layer) significant gradient of velocity and temperature are found (especially in the case of flows with heat exchange between fluid and wall). Together with the increase of the turbulent kinetic energy related to the Reynolds stress and large gradients of the mean fluid velocity, the flow becomes more turbulent.

Three sublayers can be recognized within the wall layer:

- an internal viscous sublayer, mostly influenced by molecular viscosity;
- middle transitional laminar-turbulent sublayer equally influenced by molecular viscosity and turbulence;
- outer, fully turbulent layer with dominating role of the turbulent stress.

One of the methods to model the wall layer is the use of a 'wall function', which omits calculations of the viscous sublayer where the influence of the viscosity is the greatest and only half-empirically approximates the phenomena occurring between the wall and the fully turbulent layer. Standard functions used in this paper are based upon those given by Launder and Spalding [38]. According to the so-called 'anisotropiclaw of the wall', the nondimensional velocity U^* is defined as [22]

$$U^* = \frac{1}{\kappa}\ln(Ey^*) . \tag{25}$$

In Eq. (25) one can find von Kármán constatnt $\kappa = 0.42$ and an empirical constant $E = 9.81$, whereas the nondimensional velocity U^* and nondimensional distance y^* can be expresed as

$$U^* = \frac{U_P C_\mu^{0.25} k_P^{0.5}}{\frac{\tau_w}{\rho}}, \tag{26}$$

$$y^* = \frac{\rho C_\mu^{0.25} k_P^{0.5} y_P}{\mu}, \tag{27}$$

where:

- U_P – means fluid velocity at point P (indices P at particular variables denote their values taken at point P, in a distance y of point P from the wall; index w denotes wall and f – fluid),
- k_P – turbulent kinetic energy k at point P,
- y_P – distance of point P from the wall,
- μ – dynamic viscosity,
- τ_w – wall stress.

The analogy between momentum and energy transport in the fluid leads to the similar as in Eq. (25) logarithmic relations describing temperature in the turbulent area with dominating influence of turbulence effect on the heat conduction and linear dependencies for thermal conducting sublayer, where conduction is an important process.

The law of the wall for temperature is suggested to be taken in the following form, dependent on thickness of the anisotropic thermal layer y_T^* [5]

$$T^* = \frac{(T_w - T_P)\rho c_p C_\mu^{0.25} k_P^{0.5}}{q''} = \begin{cases} \mathrm{Pr} y^* & (y^* < y_T^*) \\ \mathrm{Pr}_T \left[\frac{1}{\kappa}\ln(Ey^*) + P\right] & (y^* > y_T^*) \end{cases}, \tag{28}$$

where q'' is local heat flux and P is calculated using following relation ($A = 0.7$):

$$P = \frac{\frac{\pi}{4}}{\sin(\frac{\pi}{4})}\left(\frac{A}{\kappa}\right)^{\frac{1}{2}}\left(\frac{\mathrm{Pr}}{\mathrm{Pr}_T} - 1\right)\left(\frac{\mathrm{Pr}_T}{\mathrm{Pr}}\right)^{\frac{1}{4}}. \tag{29}$$

The molecular Prandtl number is calculated based on relation (15).

The nondimensional thickness of the thermal layer y_T^* takes the value calculated as y^* for cross-point of geometric solutions of equations expressing linear and logarithmic law of the wall for temperature [5].

4.13 Equilibrium evaporation of medium

In the classical CFD model, which has been used, there have not been taken into account the equations describing non-equilibrium formation of the new phase and that is why the classical model had to be supplemented by author's own equations, which have been created on the basis of models of nonequilibrium new phase production [4]. According to the fact that the analytical equations, describing the non-equilibrium phase transition, base on two assumptions, such as discontinuities of the medium and the other one, which is modeling using integral-derivative equations, they are not being implemented into the standard CFD codes [12].

In the CFD model, which has been used in the analysis, there has been set the equilibrium model with the assumption that there is a homogenous mixture and there is no slip between liquid and gas phase. There have also been used steam tables of given medias [3].

By thermal – FSI (fluid solid interaction) coupling, there might has been estimated increase in enthalpy of the mixture h changing phase. Therefore, the quality of the mixture has been calculated using formula:

$$x = \frac{h - h'}{h'' - h'}\,, \tag{30}$$

where:

h' – specific enthalpy of the saturated liquid at a given pressure,
h'' – specific enthalpy of dry saturated vapour at a given pressure,
h – specific enthalpy, $h = u + \frac{p}{\rho}$.

As it was mentioned before, the model used in the study assumes that the phase change supervenes in equilibrium conditions, which is totally reversible. Moreover, previously stored energy is given back without any loss. The phase change of one molecule, or a whole kilogram, occurs infinitely slowly, forming an intermediate state between saturated liquid and a saturated vapour, which is a so-called wet or moist vapour. This equilibrium intermediate state always determines the contents of the new phase. In the case of the evaporation process it is the quality x, while in case of condensation process, it is the wetness degree y.

Obviously, there occurs such a relation given under [36]:

$$x + y = 1\,. \tag{31}$$

In other words, the wet vapour found between the saturation curves is an equilibrium mixture of two phases. It might be also called a two-phase system, where vapour-liquid are in equilibrium. The entropy of such a mixture

can be calculated using formula [47]

$$\eta = (1-x)\eta' + x\eta'' \tag{32}$$

where:
η' – specific entropy of the saturated liquid at a given pressure,
η'' – specific entropy of dry saturated vapour at a given pressure.
In case of heat addition, the value of the mixture entropy will increase and the part of liquid will evaporate immediately [equilibrium]. The opposite is found during heat removal at a constant temperature, when the mixture entropy decreases and a part of steam will condensate.

4.14 Energy equation for the solid body

In analogy with Eq. (7) for the fluid, energy balance can be written also for the solid body (the wall of pipe). In the case of solving numerical problems with heat conductive solid bodies, a simple conduction equation is used which joins heat flux related to conduction with the energy flux from internal heat sources q_{int} [22]:

$$\frac{\partial}{\partial t}\rho u = \frac{\partial}{\partial x_i}\Big(\lambda \frac{\partial T}{\partial x_i}\Big) + q_{int}\,, \tag{33}$$

where u is the specific internal energy, referred to the laboratory temperature T_0,

$$u = \int_{T_0}^{T} c_v(T)dT\,. \tag{34}$$

To simplify Eq. (30), the closures are used for λ and c_ν in a form of the polynomials temperature-dependent for market available copper. The solution assumes that internal sources do not exist, thus $q_{int} = 0$.

4.15 Zero-dimensional approach

It requires noting, that the mass flow rate computed in CFD is the basic integral parameter of the 3D flow, which is controlled during the numerical process – it is possible to be read in any section A (not necessarily planar) of a turbine flow domain, oriented with a normal vector $\vec{n}$, as [3, 44]

$$\dot{m} = \int\int_A \rho\vec{v}\vec{n}dA = \bar{\rho}\bar{v}A\,, \tag{35}$$

where: $\bar{\rho}$ – average value of density; $\bar{v}$ – average value of velocity.

Heat flux, $\dot{Q}$, exchanged in finned-tube exchanger is expressed to be [3,54]:

$$\dot{Q} = \dot{Q}_{air} = \dot{Q}_{CO_2} \,, \tag{36}$$

where the air heat flux, $\dot{Q}_{air}$, is defined as

$$\dot{Q}_{air} = \dot{m}_{air}(h_3 - h_4) \,, \tag{37}$$

and the carbon dioxide heat flux $\dot{Q}_{CO_2}$ is defined as:

$$\dot{Q}_{CO_2} = \dot{m}_{CO_2}(h_2 - h_1) = \dot{m}_{CO_2}(x_2 - x_1)(h'' - h') \,. \tag{38}$$

The labels: 1, 2, 3, 4 in the Eqs. (37) and (38) refer to the Fig. 2. Points 1 and 2 are related to the phase transition of CO_2 , whereas points 3 and 4 are related to the transition of air.

5 Numerical results

As a result of discretization, over 3 million finite volume has been obtained. Heat exchanger was discretized by hexahedral structural grid, which has been refined within the boundary layer. Proper discretization of the layers is directly related to correctness of the results, as near it comes to sudden changes in the investigated parameters, in comparison to the further distance. Discretized model of the heat exchanger is shown in Fig. 3. For calculation, the finite volume method (FVM) was used and studies were carried out on previously presented model. This method leads to a stable calculation which converge relatively easily [22].

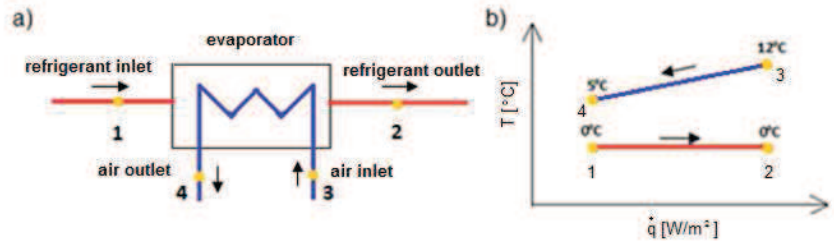

Figure 2: The principle of operation of the heat exchanger: a) scheme of exchanger; b) T-$\dot{q}$ graph of transformation in the heat exchanger.

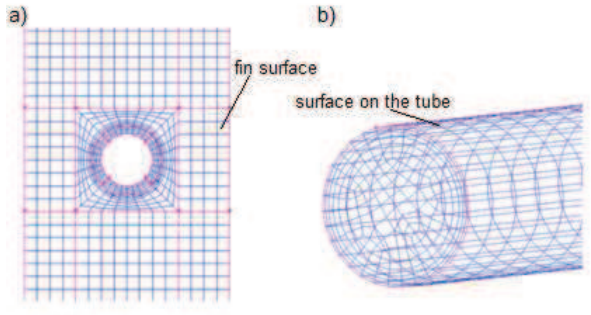

Figure 3: Discretization FVM of heat exchanger elements: a) the surface of the fins; b) the inner surface of the tube.

5.1 Analysis of mass flow rate of CO_2 and air velocity

The mass flow rate of the refrigerant in heat exchanger is assumed at levels $\dot{m}_{CO_2}$=0.04 kg/s and $\dot{m}_{CO_2}$=0.02 kg/s. While the air inlet velocity is assumed to be $\bar{v}_{air} = 5$ m/s, 6 m/s and 7 m/s.

The results of the numerical calculation obtained in commercial code are shown in Tab. 2. It can be seen that with increasing velocity of air $\bar{v}_{air}$ flowing through the heat exchanger, the temperature difference $\Delta T = T_3 - T_4$ between the inlet and outlet decreases (compare Fi. 2). Figures 4 and 5 show the temperature distribution in the fin for subsequently analyzed cases. Significant dependence of the effect of air velocity on distribution of the air temperature between fins is observed. An increase of air cooling and an increase of CO_2 vapour quality for low velocity may be clearly seen.

It should be added that the low velocity of medium is connected with low heat transfer coefficients and this will be linked directly with the CO_2 vapour quality in the outlet of evaporator (Figs. 6 and 7).

The refrigerant velocity in the cross section is directly related to mass flow rate. Increased air velocity contribute to increased mass flow rate, which directly explain the greater amount of heat flux given to the refrigerant, causing a greater vapour quality. When air velocity was $\bar{v}_{air} = 5$ m/s then CO_2 vapour quality was equal 2.3%. While air velocity increased of 2 m/s vapour quality fluctuated around 3%. The temperature distribution on the fins accepts a similar dependence like temperature of air between the fins. It can be noted that these values significantly decrease next to tubes and in the areas of the largest fluid contact, where the most intense heat transfer coefficient is achieved.

Table 2: Operating parameters obtained from numerical calculations for air velocities, respectively, $\bar{v}_{air}$ = 5 m/s, 6 m/s, 7 m/s, and the CO_2 mass flow rate m_{CO_2} = 0.04 kg/s, and 0.02 kg/s.

Operating parameters of medium							
Parameter	Symbol	Unit	Air			Carbon dioxide	
Inlet velocity	$\bar{v}$	m/s	5.00	6.00	7.00	0.767	0.384
Inlet temperature	T	K	285.00	285.00	285.00	273.00	273.00
Outlet temperature	T	K	277.70	278.12	278.46	273.00	273.00
Inlet mass flow rate	$\dot{m}$	kg/s	0.029	0.035	0.041	0.040	0.020
Inlet pressure	p_m	MPa	0.1	0.1	0.1	3.481	3.481

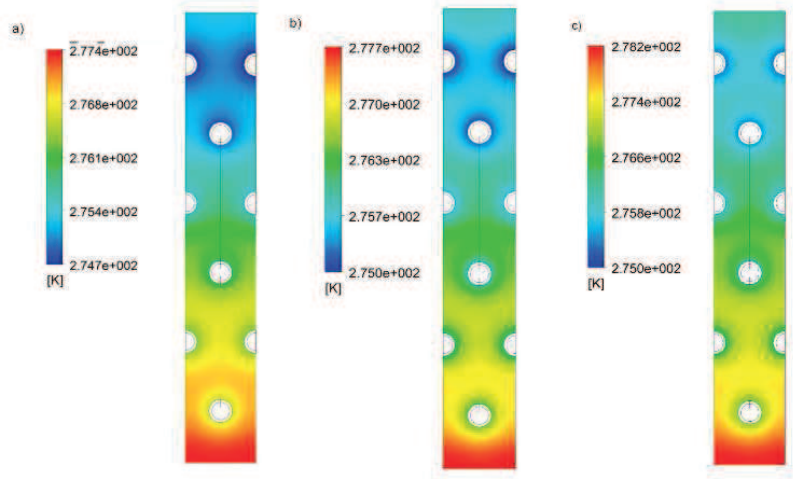

Figure 4: The temperature distribution in the fin of exchanger, with CO_2 mass flow rate $\dot{m}_{CO_2}$ = 0.04 kg/s, and for air inlet velocity: a) 5 m/s, b) 6 m/s, c) 7 m/s.

5.2 Heat exchanger characteristic

In Tables 3 and 4 are listed basic values of researched heat exchanger, i.e., heat flux of heat exchange and coefficients of heat transfer on both (air and CO_2) side. Figures 8 and 9 present the influence of air mass flow rate $\dot{m}_{air}$ in the heat exchanger, respectively, on the heat flux $\dot{Q}$ of this device and on the size of the heat transfer coefficient, at constant refrigerant mass flow rate.

As can be seen in Fig. 8, heat flux $\dot{Q}$ increases proportionally with the

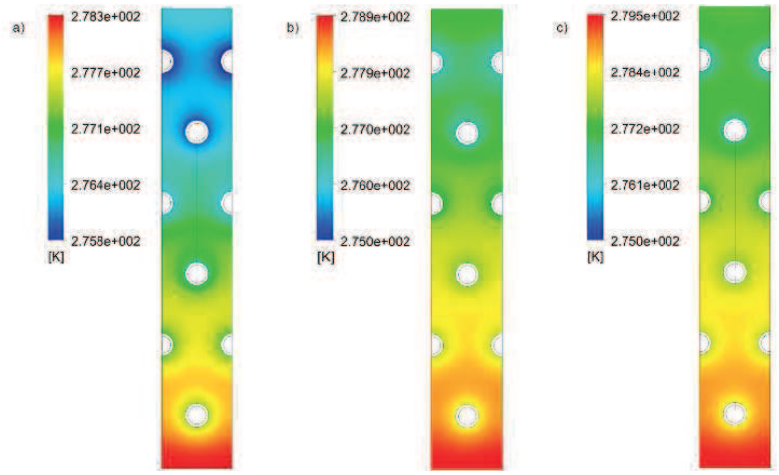

Figure 5: The temperature distribution in the fin of exchanger, with CO_2 mass flow rate $\dot{m}_{CO_2} = 0.02$ kg/s, and for air inlet velocity: a) 5 m/s, b) 6 m/s, c) 7 m/s.

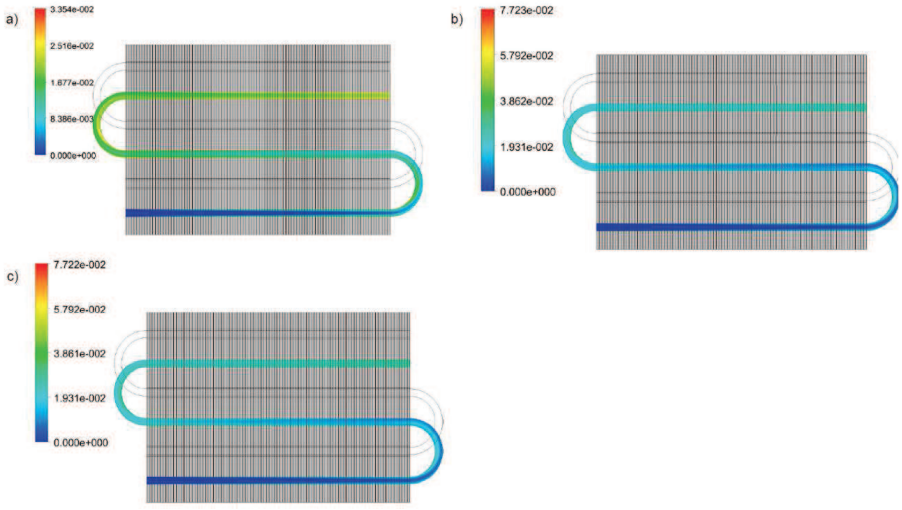

Figure 6: Refrigerant vapour quality coefficient in heat exchanger with CO_2 mass flow rate $\dot{m}_{CO_2}$=0.04 kg/s, and for airinlet velocity: a) 5 m/s, b) 6 m/s, c) 7 m/s.

increase of air mass flow rate and with the drops of air temperature decrease. Differences of air temperature are higher and denote its lower outlet temperature. Lower air outlet temperature occurs for the lower velocity, which is associated with prolonged contact with the heat exchange medi-

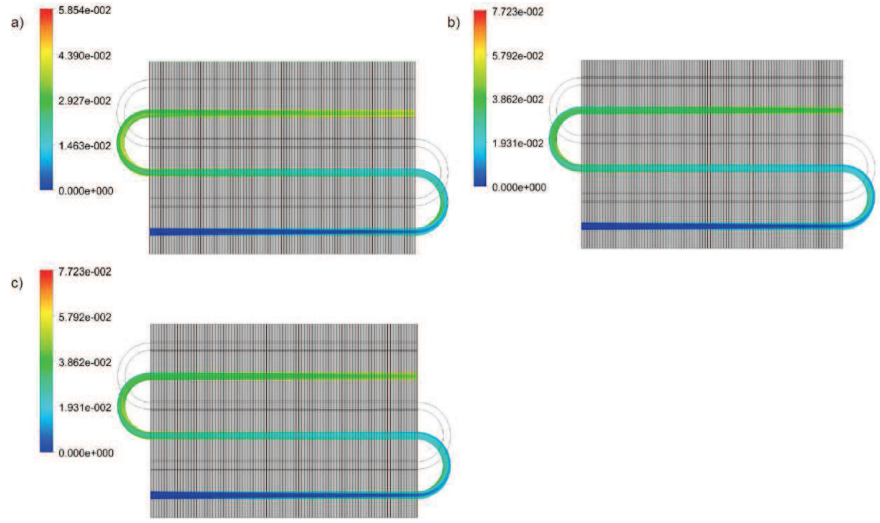

Figure 7: Refrigerant vapour quality coefficient in heat exchanger with CO_2 mass flow rate $\dot{m}_{CO_2}$=0.02 kg/s, and for airinlet velocity: a) 5 m/s, b) 6 m/s, c)7 m/s.

ums. Reduction of the refrigerant mass flow rate does not show changes in tendency, but the values of heat flux and air drop are lower.

Table 3: Dependence of the heat flux and the heat transfer coefficient on the air flow rate m_{air}, at a constant mass flow rate of CO_2 m_{CO_2} = 0.04kg/s.

Parameter	Symbol	Unit	Value of parameter		
The mass flow rate of the refrigerant	$\dot{m}_{CO_2}$	[kg/s]	0.04		
The mass flow rate of air	$\dot{m}_{air}$	kg/s	0.029	0.035	0.041
Air temperature decrease	ΔT	K	7.30	6.88	6.54
Heat flux	$\dot{Q}$	W	211	239	264
Heat transfer coefficient on the air side	α_{air}	W/(m^2 K)	110.68	116.68	132.85
Heat transfer coefficient on the CO_2 side	α_{CO_2}	W/(m^2 K)	3483.22	3452.21	3425.70

As seen in the next graph (Fig. 9), with the increase of the air mass flow rate $\dot{m}_{air}$ the heat transfer coefficient at the air side, α_{air}, increases, while at the side of the refrigerant, α_{CO_2}, decreases and shows its dependence from amount of CO_2 mass flow rate $\dot{m}_{CO_2}$. It can also be noted that the heat transfer coefficients not only depend on the temperature distribution

Table 4: Dependence of the heat flux and the heat transfer coefficient on the air flow rate m_{air}, at a constant mass flow rate of CO_2 $m_{CO_2} = 0.02$ kg/s.

Parameter	Symbol	Unit	Value of parameter		
The mass flow rate of the refrigerant	$\dot{m}_{CO_2}$	kg/s	0.02		
The mass flow rate of air	$\dot{m}_{air}$	kg/s	0.029	0.035	0.041
Air temperature decrease	ΔT	K	6.29	5.92	5.51
Heat flux	$\dot{Q}$	W	184	204	221
Heat transfer coefficient on the air side	α_{air}	W/(m^2 K)	110.63	116.60	132.71
Heat transfer coefficient on the CO_2 side	α_{CO_2}	W/(m^2 K)	2006.68	1986.55	1968.90

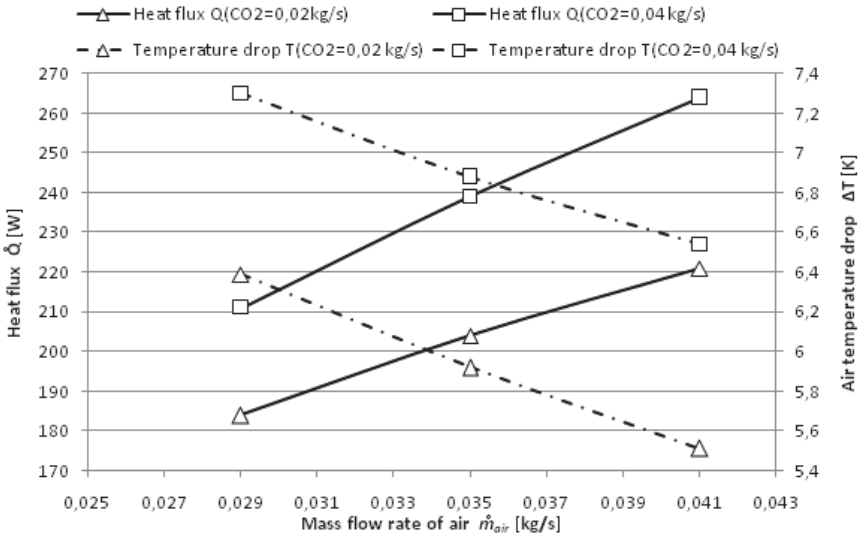

Figure 8: Dependence of the heat flux and air temperature drop on air mass flow rate at a constant mass flow rate of refrigerant.

in the fluid (mainly in the boundary layer) and on the fluid flow conditions, but also on the thermal conductivity of the fluid. These results confirm the proper selection of medium to the type of heat exchanger, because finned-tube heat exchangers have low heat transfer coefficients on one side ($\alpha_{air} = 100 \div 135$)and a much higher on the other side.

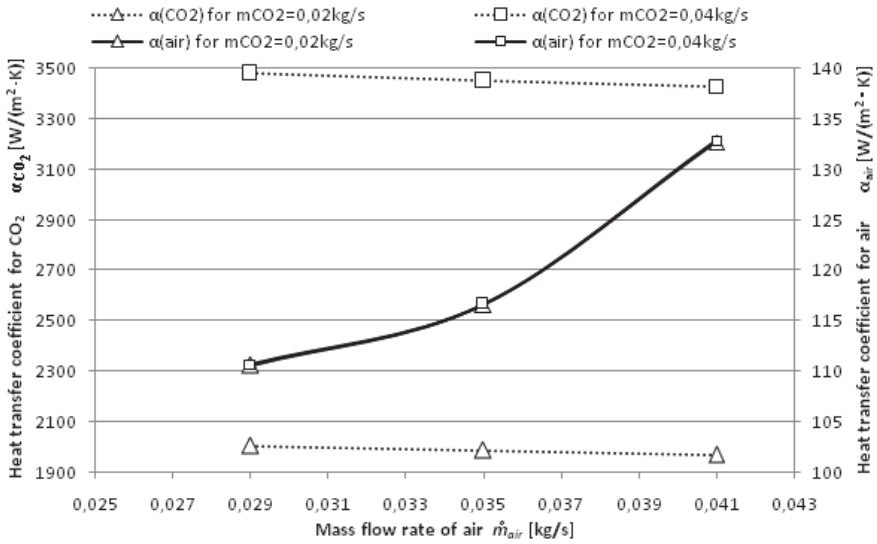

Figure 9: Dependence of the heat transfer coefficient on air mass flow rate at a constant flow of refrigerant.

6 Conclusions

As a result of conducted study, the characteristic of heat exchanger with CO_2 was obtained. Numerical analysis of tested heat exchanger, used as an evaporator, was carried out basing on equations of mass, momentum and energy conservation to calculate a finite volumes. On the air and medium side, heat transfer coefficients, α, heat flux, $\dot{Q}$, and temperature drop, ΔT, was obtained directly from the calculation as the average values along the circumference.

Heat flux $\dot{Q}$ of heat exchanger has significantly dependence on both the refrigerant $\dot{m}_{CO_2}$ and the air mass flow rate $\dot{m}_{air}$. Increase in the velocity of refrigerant causes less temperature drops, which has an influence on the temperature distribution on the fins and on the vapour quality, x, of the refrigerant in the tubes. Heat transfer coefficients on the air side, α_{air}, shows significantly dependents on its velocity $\bar{v}_{air}$ and slight dependence on the amount of refrigerant $\dot{m}_{CO_2}$. Heat transfer coefficients on the side of CO_2 α_{CO_2} have strong dependence on both parameters.

Excessive velocity of air could cause noise. We should select appropriate operating parameters and remember about the possibility of controlling

the flow of the heat exchangers. High values of heat transfer coefficient α indicate a very good grade of heat exchange. However, the increase in heat transfer coefficient α is usually associated with an increase of flow resistance and high pressure drop Δp in the heat exchanger. Thus, the optimal quantity of heat transfer coefficients and the quantity of the flow resistance should to be found, because this translates into economic aspects.

Plates arrangement and the velocity of the air inlet to finned-tube heat exchangers should be adjusted according to the quantity of the heat exchanger, to air outlet conditions and to the required capacity, which aim is to achieve better performance. Hence, these exchangers should be also provided with a system parameter adjustment of inlet coefficient. Heat exchangers should be designed in a way that their material consumption was as low as possible. This is achieved, inter alia, by selection of the appropriate exchanger, used with the proper organization of flow coefficient to data type of heat exchanger. Currently, a modern solution is microchannels heat exchangers, having lower heat exchange surfaces and higher heat transfer coefficients. Thus, the analysis of the heat exchange between the coefficients discussed in the microchannels should be considered.

Received 11 March, 2015

References

[1] Abdulsayid A.: *Modeling of fluid flow in 2D triangular, sinusoidal, and square corrugated channels.* World Academy of Science, Eng. Technol. **71**(2012), 34–52.

[2] Austin B.T., Sumathy K.: *Transcritical carbon dioxide heat pump systems: a review.* Elsevier, Renew. Sust. Energ. Rev. **15**(2001), 4013–4029.

[3] Badur J.: *Five lecture of contemporary fluid termomechanics.* Gdańsk 2005. (in Polish).

[4] Badur J., Banaszkiewicz M.: *Model of the ideal fluid with scalar microstructure. An application to flashing flow of water.* Transactions IFFM **105**(1999), 115–152.

[5] Badur J.,Charun H.: *Selected problems of heat exchange modelling in pipe channels with ball turbulisers.* Arch. Thermodyn. **28**(2007), 1, 65–87.

[6] Badur J., Ziółkowski P.: *Further remarks on the surface visimperssa caused by a fluid-solid contact.* In: Proc. 12th Joint European Thermodynamics Conf., Brescia July 1–6, 2013, 581–586.

[7] Badur J., Ziółkowski P., Zakrzewski W., Sławiński D., Kornet S., Kowalczyk T., Hernet J., Piotrowski R., Felicjancik J., Ziółkowski P.J.: *An advanced Thermal–FSI approach to flow heating/cooling.* J. Phys.: Conf. Ser. **530**(2014), 10.1088/1742–6596/530/1/012039.

[8] Banaszek J., Rebow M.: *Reliability of numerical simulation in composed heat exchange.* In: Proc. 18th Thermodynamics Cong. Vol. I, Warsaw 2002, p. 45 (in Polish).

[9] Bartosiewicz J., Bogusławski L., Wróblewska A.: *Numerical analysis of heat transport in channels with embossed intensifiers.* In: Proc. 18th Thermodynamics Cong. Vol. I, Warsaw 2002, p. 67.

[10] Bejan A.: *Entropy Generalization Minimization.* Boca Raton: CRC, 1996.

[11] Bejan A, Kraus A.D.: *Heat Transfer Handbook.* Wiley & Sons, Hoboken 2003.

[12] Bilicki Z., Badur J.: *A thermodynamically consistent relaxation model for a turbulent, binary mixture undergoing phase transition.* J. Non-Equil. Thermody. **28**(2003), 145–172.

[13] Bilicki Z., Mikielewicz J.: *Minimum energy and a minimum of entropy production in application to calculate the filling level in a two-phase bubble flow.* Arch. Thermodyn. **5**(1984), 84, 101–118 (in Polish).

[14] Bogusławski L.: *Turbulence modelling in non-izothermic flows.* Scientific Papers of Łódź University of Technology **197**(1988), 558, 101–122. (in Polish)

[15] Bonca Z., Butrymowicz D., Targański W., Hajduk T.: *Guide, New refrigerants and heat medium. Thermal, chemical and usable properties.* IPPU MASTA, 2004. (in Polish).

[16] Cano-Andrade S., Beretta G. P., von Spakovsky M. B.: *Non-equilibrium thermodynamics modelling of an atom-field state evolution with comparisons to published experimental data.* In: Proc. 12th Joint European Thermodynamics Conf., Brescia July 1–6, 2013, 430–436.

[17] Charun H.: *Comparatory research of convective heat exchange intensification with ball turbulizers.* Ciepłownictwo, Ogrzewnictwo, Wentylacja **1**(2005), 3–8 (in Polish).

[18] Fang X., Zhou Z., Li D..: *Review of correlations of flow boiling heat transfer coefficients for carbon dioxide.* Int. J. Refrig. (2013). Doi: 10.1016/j.ijrefrig.2013.05.015.

[19] Feidt M.: *Thermodynamics of energy systems; a review and perspectives.* J. Appl. Fluid Mech. **5**(2012), 2, 85–98.

[20] Feidt M.: *Energy engineering: From components design to intergration and control system.* Dunod, Paris 2014

[21] Fernandes C., Dias R., Nobrega J., Maia J.: *Laminar flow in chevron-type plate heat exchangers: CFD analysis of tortuosity, shape factor and friction factor.* Chem. Eng. Process. **46**(2007), 825–833.

[22] Ferziger J.H., Perić M.: *Computatonal Methods for Fluid Dynamics.* Springer, Berlin 1999.

[23] Fodemski T.R., Plocek M.: *Analysis of characteristics of thermo-flow installations selected elements based on measurements and numerical simulation (using CFX-Flow 3D code).* In: proc. 10th Symp. of Heat and Mass Transfer, Wrocław 1998, 242–247 (in Polish).

[24] Gherasim I., Galanis N., Nguyen C.: *Effects of smooth longitudinal passages and port configuration on the flow and thermal fields in a plate heat exchanger.* Appl. Therm. Eng. **31** (2011), 4113–4124.

[25] Gherasim I., Galanis N., Nguyen C.: *Heat transfer and fluid flow in a plate heat exchanger. Part II: Assessment of laminar and two-equation turbulent models.* Int. J. Therm. Sci. **50**(2011), 1499–1511.

[26] Gherasim I., Taws M., Galanis N., Nguyen C.: *Heat transfer and fluid flow in a plate heat exchanger. Part I. Experimental investigation.* Int. J. Therm. Sci. **50**(2011), 1492–1498.

[27] Gryboś R.: *Rudiments of fluid mechanics.* PWN, Warsaw 1998 (in Polish).

[28] Gyftopoulos E.P., Beretta G.P.: *Thermodynamics Foundations and Applications.* Dover Pub. Mineola NY, 2005.

[29] Heo J., Park H., Yun R.: *Condensation heat transfer and pressure drop characteristics of CO_2 in a microchannel.* Int. J. Refrig. 09/2013, 36(6), 1657-1668. DOI: 10.1016/j.ijrefrig.2013.05.008.

[30] Jin Z., Park G., Lee Y., Choi S., Chung H., Jeong H.: *Design and performance of pressure drop and flow distribution to the channel in plate heat exchanger.* In: Proc. EngOpt 2008 – Int. Conf. Engineering Optimization, Rio de Janeiro, June 01–05, 2008.

[31] Kanaris A.G., Mouza A.A., Paras S.V.: *Optimal design of a plate heat exchanger with undulated surfaces.* Int. J. Therm. Sci. **48**(2009), 1184–1195.

[32] Karaszkiewicz E.: *The Outline of the Vector and Tensor Theory.* PWN, Warsaw 1976 (in Polish).

[33] Karcz M., Badur J.: *An alternative two-equation turbulent heat diffusivity closure.* Int. J. Heat Mass Tran. **48**(2005), 2013–2022.

[34] Kazimierski Z.: *Numerical solving of three-dimensional turbulent flows.* Ossolineum, Wrocław-Warszawa-Kraków 1992 (in Polish).

[35] Klaczak A.: *Spiral turbulizers usability in heat exchanger reinforcment and bulding.* Ciepłownictwo Ogrzewnictwo Wentylacja **7**(1971) p. 197 (in Polish).

[36] Kornet S., Badur J.: *Non-equilibrium phase transition.* Logistyka **4**(2012), 225–233.

[37] Kowalczyk S., Karcz M., Badur J.: *Analysis of thermodynamic and material properties assumptions for three-dimensional SOFC modeling.* Arch. Thermodyn. **27**(2006), 21–38.

[38] Launder B.E., Spalding D.B.: *The numerical computation of turbulent flows.* Comput. Methods Appl. M. Eng. **3**(1974), 2, 269–292.

[39] Lin K.-H., Kuo C.-S., Hsieh W.-D., Wang C.-C.: *Modeling and simulation of the transcritical CO_2 heat pump system.* Int. J. Refrig. (2013). DOI: 10.1016/j.ijrefrig.2013.08.008.

[40] Madejski J.: *Theory of Heat Transfer.* Szczecin University of Technology, Szczecin 1998 (un Polish).

[41] Madejski P., Taler D.: *Analysis of temperature and stress distribution of superheater tubes after attemperation or sootblower activation.* Energ. Convers. Manage. **71**(2013), 131–137.

[42] Martinez-Ballester S., Corberan J., Gonzalvez-Macia J.: *Numerical model for microchannel condensers and gas coolers: Part I – Model description and validation.* Int. J. Refrig. **36**(2013), 173–190.

[43] Martinez-Ballester S., Corberan J., Gonzalvez-Macia J.: *Numerical model for microchannel condensers and gas coolers: Part II – Simulation studies and model comparison.* Int. J. Refrig. **36**(2013), 191–202.

[44] Nastałek L., Karcz M., Sławiński D., Zakrzewski W., Ziółkowski P., Szyrejko C., Topolski J., Werner R., Badur J.: *On the internal efficiency of a turbine stage: classical and computational fluid dynamics definitions.* Transactions IFFM **124**(2012), 17–39.

[45] Rup K., Wais P.: *A k-ε model with variable Prandtl number.* In: Proc. 10th Symp. of Heat and Mass Transfer, Wrocław 1998, Part 2, 777–783 (in Polish).

[46] Sanaye S., Dehghandokht M.: *Thermal modeling of mini-channel and laminated types evaporator in mobile air conditioning system.* Int. J. Automotive Eng. **2**(2012), 2, 68–83.

[47] Schnerr H., Badur J.: *Multiphase flows and problems related to the condensation and cavitation processes.* Rep. IFFM PASci 23/02, Gdańsk 2002, 1–44.

[48] Taler D., Ocłoń.: *Thermal contact resistance in plate finned-and-tube heat exchangers, determined by experimental data and CFD simulations.* Int. J. Therm. Sci. **84**(2014), 309–22.

[49] Taler J., Duda P., Węglowski B., Zima W., Grądziel S., Sobota T., Taler D.: *Identification of local heat flux to membrane water-walls in steam boilers.* Fuel **88**(2009), 305–11.

[50] Valencia A., Cid M.: *Turbulent unsteady flow and heat transfer in channel with periodically mounted squary bars.* Int. J. Heat Mass Tran. **45**(2002) 1661–1673.

[51] Wiśniewski S.: *Application of numerical method in convective heat exchange research.* Scientific Papers of Łódź University of Technology **197**(1998), 558, 191–204 (in Polish).

[52] Wiśniewski S., Wiśniewski T.: *Heat Transfer.* WNT, Warsaw 1994 (in Polish).

[53] Ziółkowski P., Badur J.: *Navier number and transition to turbulence.* J. Phys.: Conf. Ser. **530**(2014), 012035.

[54] Ziółkowski P., Badur J.: *Clean gas technologies towards zero-emission repowering of Pomerania.* Transactions IFFM **124** (2012), 51–80.